JOURNAL OF GEOPHYSICAL RESEARCH, VOL. 112, D12102, doi:10.1029/2006JD007878, 2007

Toward understanding the double Intertropical Convergence Zone pathology in coupled ocean-atmosphere general circulation models

Xuehong Zhang,[1] Wuyin Lin,[2] and Minghua Zhang[2]

Received 3 August 2006; revised 22 January 2007; accepted 27 February 2007; published 16 June 2007.

[1] This paper first analyzes structures of the double Intertropical Convergence Zone (ITCZ) in the central equatorial Pacific simulated by three coupled ocean-atmosphere general circulation models in terms of sea surface temperatures, surface precipitation, and surface winds. It then describes the projection of the double ITCZ in the equatorial upper ocean. It is shown that the surface wind convergences, associated with the zonally oriented double rainbands on both sides of the equator, also correspond to surface wind curls that are favorable to Ekman pumping immediately poleward of the rainbands. The pumping results in a thermocline ridge south of the equator in the central equatorial Pacific, causing a significant overestimation of the eastward South Equatorial Counter Current that advects warm water eastward. A positive feedback mechanism is then described for the amplification of the double ITCZ in the coupled models from initial biases in stand-alone atmospheric models through the following chain of interactions: precipitation (atmospheric latent heating), surface wind convergences, surface wind curls, Ekman pumping, South Equatorial Counter Current, and eastward advection of ocean temperature. This pathology provides a possible means to address the longstanding double ITCZ problem in coupled models.

Citation: Zhang, X., W. Lin, and M. Zhang (2007), Toward understanding the double Intertropical Convergence Zone pathology in coupled ocean-atmosphere general circulation models, *J. Geophys. Res.*, *112*, D12102, doi:10.1029/2006JD007878.

1. Introduction

[2] Double Intertropical Convergence Zone (ITCZ), defined in rainfall, is a common problem in coupled atmosphere-ocean models without flux corrections [*Mechoso et al.*, 1995; *Meehl and Arblaster*, 1998; *Terray*, 1998; *Kirtman et al.*, 2002; *Guilyardi et al.*, 2003; *Kiehl and Gent*, 2004]. Many previous studies have focused on the double ITCZ in the Eastern Pacific (100°W–150°W) where models tend to simulate two rainbands on both sides of the Equator throughout the year, while in observations the rainband south of the Equator only appears in the boreal spring season [*Zhang*, 2001]. The spurious rainbands in the south have been shown to relate to warm biases of sea surface temperatures (SST) in the Southeast Pacific due to deficient amount of low clouds in the models [*Ma et al.*, 1996; *Yu and Mechoso*, 1999; *Dai et al.*, 2003].

[3] Coupled models also tend to simulate double ITCZ in the western and central equatorial Pacific (160°E to 140°W). There in observations, the ITCZ north of the Equator and the South Pacific Convergence Zone (SPCZ) form an asymmetric precipitation pattern [*Waliser*, 2003]. In models, however, the simulated SPCZ is typically symmetric to the ITCZ in the north. It is sometimes referred to as the South Convergence Zone (SCZ) because of its significant differences from the observed SPCZ [e.g., *Guilyardi et al.*, 2003]. Since most coupled models can simulate the ITCZ north of the Equator reasonably well, the double ITCZ bias is primarily a feature in the south equatorial Pacific [*Covey et al.*, 2003].

[4] An associated problem with double ITCZs in coupled models is the westward extension of the cold tongue from the eastern equatorial Pacific. Because of the extended cold tongue, simulated sea surface temperatures in the western equatorial Pacific are much lower than observations [*Mechoso et al.*, 1995; *Latif et al.*, 2001; *Davey et al.*, 2002].

[5] The objective of the paper is to offer insight into the pathology of the double ITCZ in coupled models by understanding the physical processes. We first compare simulations from three coupled ocean-atmosphere models against available observations by analyzing their doubled ITCZ structures in the western and central equatorial Pacific in terms of SST, precipitation and surface winds. These biases are then projected to the upper ocean in terms of thermocline structures and equatorial currents and compared with observations. On the basis of these structures, we propose a mechanism of how double ITCZ in coupled models develop through a positive feedback mechanism that eventually leads to a symmetric structure of the atmospheric and oceanic characteristics about the Equator.

2. Models and Data

[6] Annual climatological simulations from three coupled ocean-atmosphere general circulation models are used in

[1]State Key Laboratory of Atmospheric Sciences and Geophysical Fluid Dynamics, Institute of Atmospheric Physics, Chinese Academy of Sciences, Beijing, China.

[2]Institute for Terrestrial and Planetary Atmospheres, Stony Brook University, State University of New York, Stony Brook, New York, USA.

0148-0227/07/2006JD007878$09.00

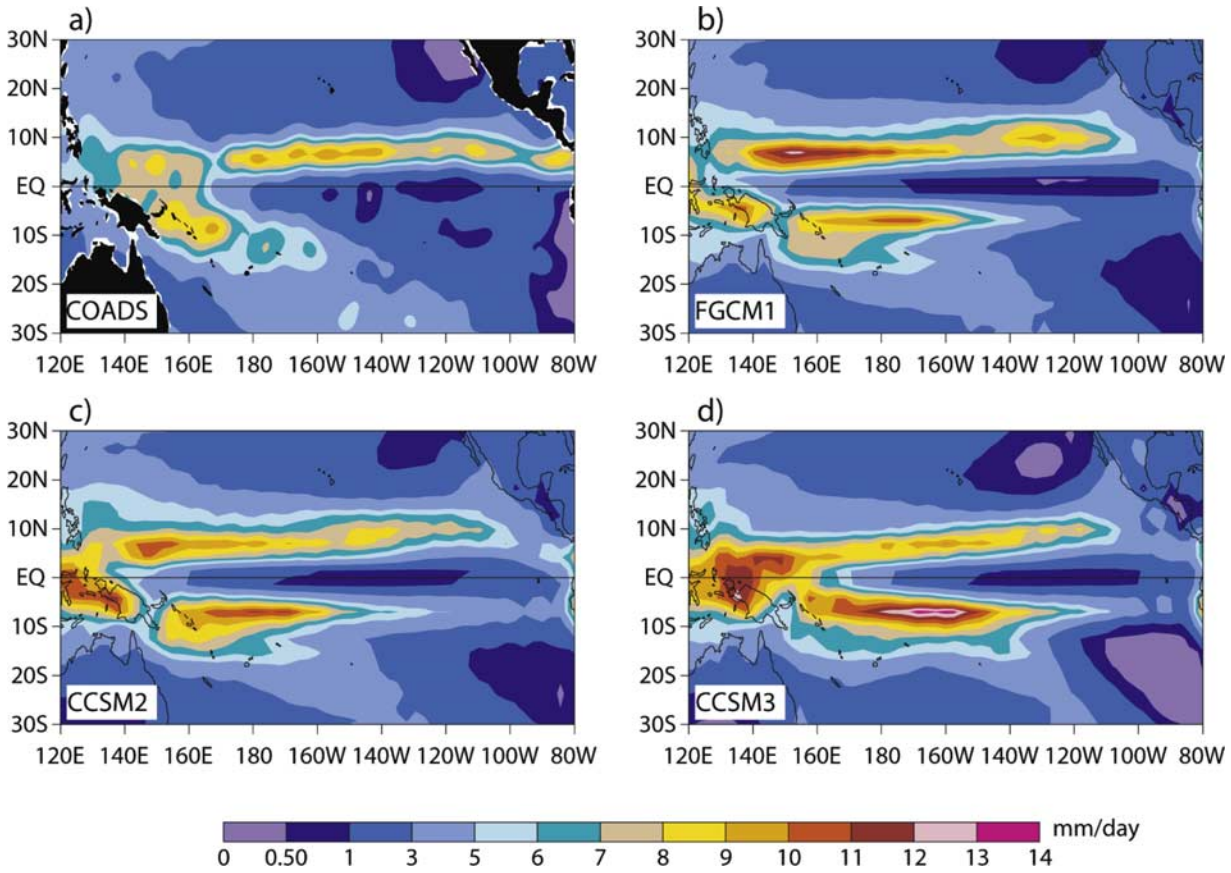

Figure 1. Annual mean precipitation rates (mm/d) from (a) COADS, (b) FGCM-1, (c) CCSM2, and (d) CCSM3.

this study. The models are the Laboratory of Numerical Modeling for Atmospheric Sciences and Geophysical Fluid Dynamics/Institute of Atmospheric Physics (LASG/IAP) Flexible coupled General Circulation Model (FGCM) version one (referred to as FGCM-1) [*Yu et al.*, 2005], the NCAR Community Climate System Model, version two (CCSM2) [*Kiehl and Gent*, 2004], and version three (CCSM3) [*Collins et al.*, 2005].

[7] The FGCM-1 is formulated on the basis of the CCSM2 by replacing the CCSM2's ocean component CCSM2 POP [*Smith and Gent*, 2002] with the LASG/IAP Climate Ocean Model version 1.0 (referred to as LICOM1.0) [*Liu*, 2002], by virtue of the CCSM2's flux coupler. All the other components of CCSM2, particularly the atmospheric component, Community Atmospheric Model, version two (CAM2), are not changed in the FGCM-1. The coupling domains are 75°S–65°N for FGCM-1 and global for CCSM2 and CCSM3. The differences between the CCSM2 and CCSM3 are described by *Collins et al.* [2005]. We therefore have two atmospheric GCMs (CAM2 and CAM3 for CCSM2 and CCSM3, respectively) and three oceanic GCMs in the three coupled models, which are used to analyze the common model biases. The CCSM2 and CCSM3 simulations are averages of years 961–980 and years 701–720, respectively from 1000 years of control simulations (experiments b20.007 and b30.004, http://www.ccsm.ucar.edu/experiments/). The results shown in the paper are found to be similar for other averaging period. For the FGCM1, averages for years 101 to 130 were used from a 150 year simulation that branched from a longer control simulation.

[8] The climatological precipitation and surface wind stress data of COADS [*da Silva et al.*, 1994] and the ocean temperature and current velocity data of the NCEP Ocean Data Assimilation System (referred to as NCEP ODAS) [*Ji et al.*, 1995; *Behringer et al.*, 1998] are used in this study to compare with model simulations.

3. Results

3.1. Symmetry in the Modeled SPCZ-ITCZ Structure

[9] Figure 1 shows the annual climatological precipitation from observations and the three coupled models. There are many similarities among the models in the precipitation pattern in the equatorial Pacific, which are different from observations. The most conspicuous feature is that east of 150°W between 5°S to 10°S, the models simulated stronger precipitation than observation. The excess precipitation in this region is already less severe than those in earlier studies [*Meehl and Arblaster*, 1998; *Yu et al.*, 2002]. In observation, the SPCZ rainband has a northwest-southeast orientation starting from eastern Papua New Guinea to around (120°W, 30°S); rainfall maximum of 6 mm/d extends as far south as 15°S near 160°W. In contrast, the simulated SPCZ extends eastward zonally within 10 degrees of the equator in the models, with a narrow band maximum rainfall of over

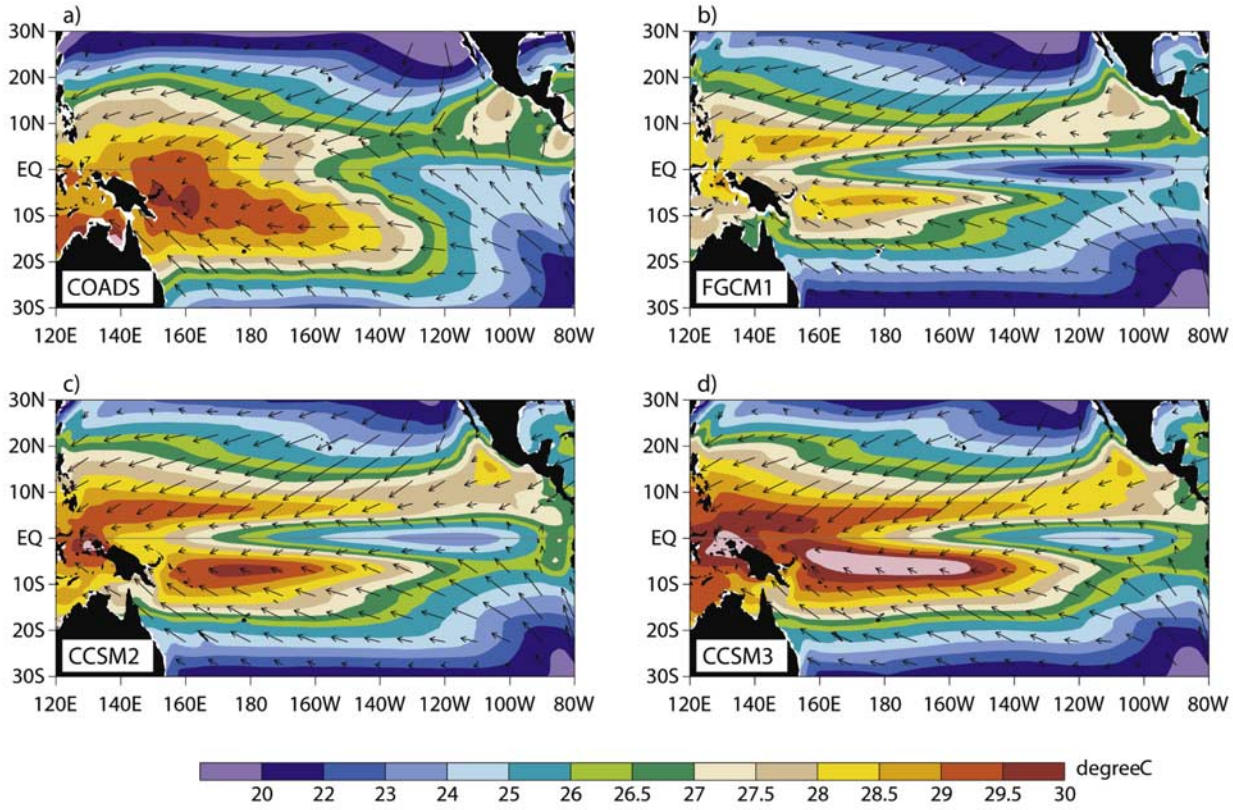

Figure 2. Annual mean SST (°C) and surface wind stress vector from (a) COADS, (b) FGCM-1, (c) CCSM2, and (d) CCSM3.

10 mm/d between 5°S and 10°S in the central equatorial Pacific around 160°W.

[10] A second problem with the simulated precipitation is the westward extension of the dry zone along the equator, in particular in FGCM-1 and CCSM2, which effectively cuts off the observed connection between the ITCZ north of the Equator and the SPCZ south of the Equator. As a result, all models simulated a highly symmetric SPCZ and ITCZ to the Equator. This feature is common to the majority of coupled models [*Mechoso et al.*, 1995; *Latif et al.*, 2001; *Davey et al.*, 2002].

[11] The symmetric structure of the ITCZ is also accompanied by two maximum sea surface temperature (SST) bands and a westward extension of the cold tongue (Figure 2) in the models. The models tend to show a warm SST bias north and south of the equator in the eastern equatorial Pacific. The models also simulated very different warm pool SSTs, with the FGCM1 significantly cooler than observation, while CCSM3 warmer than observation. The most prominent feature of the models, common to coupled models, is the spurious double ITCZ in convection distribution. Because of this, coupled models tend to have frequent "aborted ENSO (El Nino–Southern Oscillation)" [*Guilyardi et al.*, 2003, pp. 1141–1158], and overestimate the ENSO signals in the western and central equatorial Pacific and their relationships with the Asian monsoons [*Latif et al.*, 2001; *Kiehl and Gent*, 2004].

[12] The double ITCZs in the models also correspond to convergences of the surface winds (Figure 2). In observations, the southward surface wind component in the SPCZ is mainly from the counterclockwise deflection of the southeast trade wind in the central South Pacific [*Tomczak and Godfrey*, 2001]. This wind component contributes to the convergence in the SPCZ. In the models, winds with southerly components are located between 7°S to 10°S, well north of the transition latitude in the observation. The meridional wind component is restricted to a narrow zonal band in the western and central equatorial Pacific. It diverges from the Equator toward the two rainbands off the Equator. The surface wind convergence pattern is therefore a mirror image of the precipitation and SST patterns. Figure 2 also shows that the models tend to simulate too strong southeast trade winds in the central South Pacific around 10°S between 180°W–140°W, which are also much closer to the equator than that in observations. The divergent winds away from the equator and the northward shift of the southeast trade winds both contribute to the model SPCZ structure that is too zonal and too strong in the central equatorial Pacific.

[13] These biases in the SST, precipitation, and surface winds are related to each other through the well known interactions within the tropical atmosphere: high SSTs in the central equatorial Pacific cause more convection and thus more precipitation; the latent heating associated the excessive precipitation corresponds to stronger convergence of surface winds [e.g., *Zhang*, 1996]. In the following, we show that these components further project into biases in the

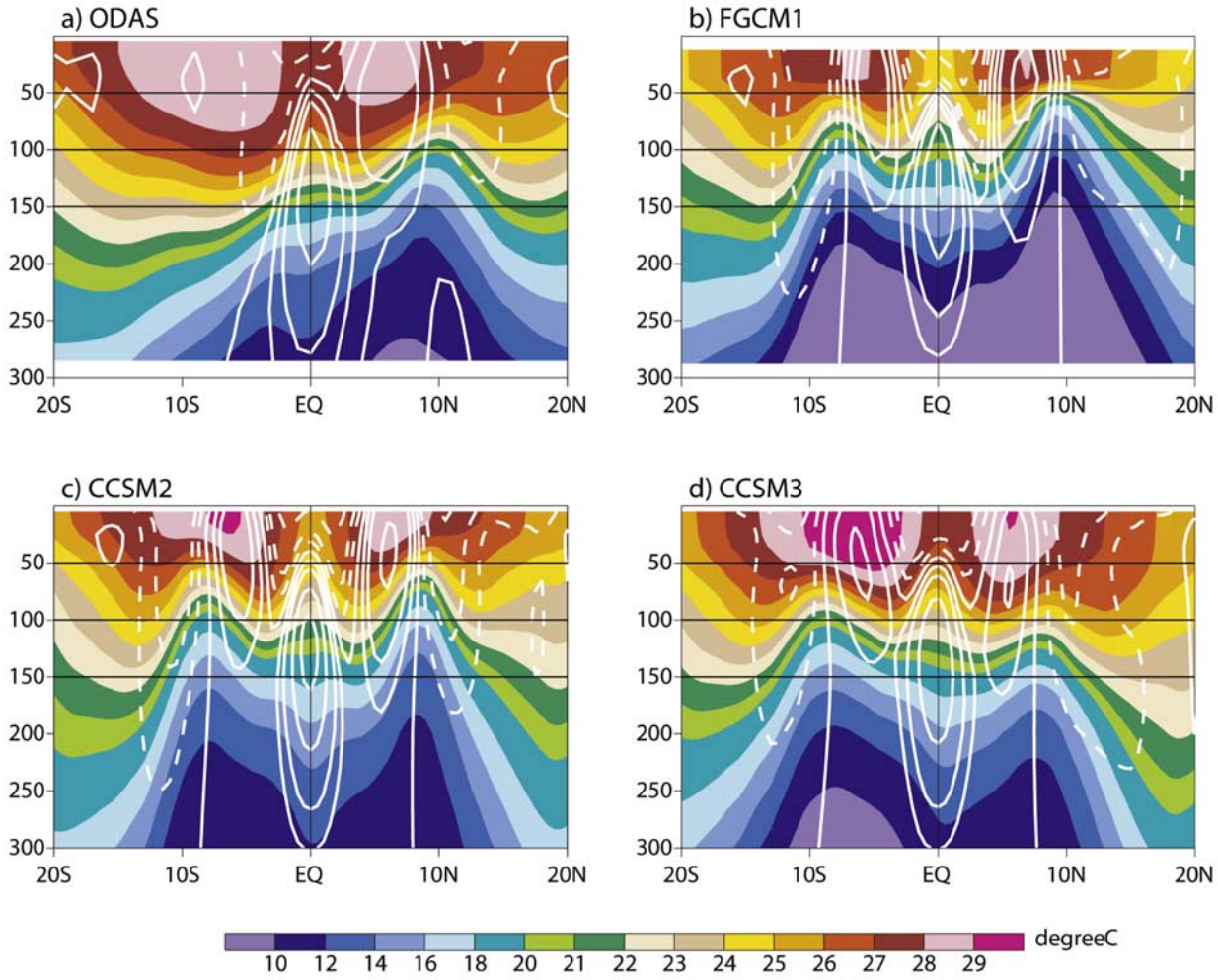

Figure 3. Latitude-depth diagram of annual mean oceanic temperature (shaded, in °C) and zonal current (white contours, eastward in solid and westward in dashed lines), averaged over 160°E–140°W for (a) NCEP ODAS, (b) FGCM-1, (c) CCSM2, and (d) CCSM3.

ocean currents that can positively feedback and thus amplify an initial bias in the SSTs in the central equatorial Pacific.

3.2. Symmetric Ridging of the Thermocline and Bias in the Equatorial Ocean Currents

[14] Figure 3 shows the cross section of upper ocean temperatures and zonal currents in the western and central Pacific averaged from 160°E to 140°W calculated from NCEP ODAS, FGCM-1, CCSM2, and CCSM3. Results from NCEP ODAS are very similar to the earlier observational analysis of *Kessler and Taft* [1987]. A distinct feature in the observation is the asymmetry of thermocline and the zonal currents to the equator. Near 10°N, immediately north of the ITCZ, there is a strong subsurface ridge of the thermocline. This is the result of strong upwelling. Near 10°S, the thermocline ridge is very weak. As a result, the thermocline slopes up gradually from 10°S to 10°N. The depth of the 20°C isotherm is about 200 m near 10°S. It becomes 120 m at 10°N. The subsurface water temperature south of the Equator is much warmer than that in the north. The warm pool south of the Equator is thicker and broader than its counterpart in the north, with the maximum temperature more than 1°C higher.

[15] The opposite signs of the thermocline slope on the two sides of 10°N in the ODAS analysis correspond to a trough in the sea surface height at this latitude. North of it is the westward North Equatorial Current (NEC), and south of it is the eastward North Equatorial Counter Current (NECC) (Figure 3a). The southern edge of the subsurface NECC connects to the eastward Equatorial Undercurrent (EUC). In contrast, South of the Equator, the westward South Equatorial Current (SEC) dominates. The observed South Equatorial Counter Current (SECC) is much weaker than the NECC. It is displaced poleward and therefore it does not connect with the EUC.

[16] In the FGCM-1, CCSM2, and CCSM3, Figures 3b–3d show that the simulated structures of the thermocline and the zonal currents north of the Equator are similar to NCEP ODAS calculations. South of the Equator, however, the models all have structural biases. A spurious thermocline ridge appears at about 10°S in all models that corresponds to the distorted structures of the simulated SPCZ discussed

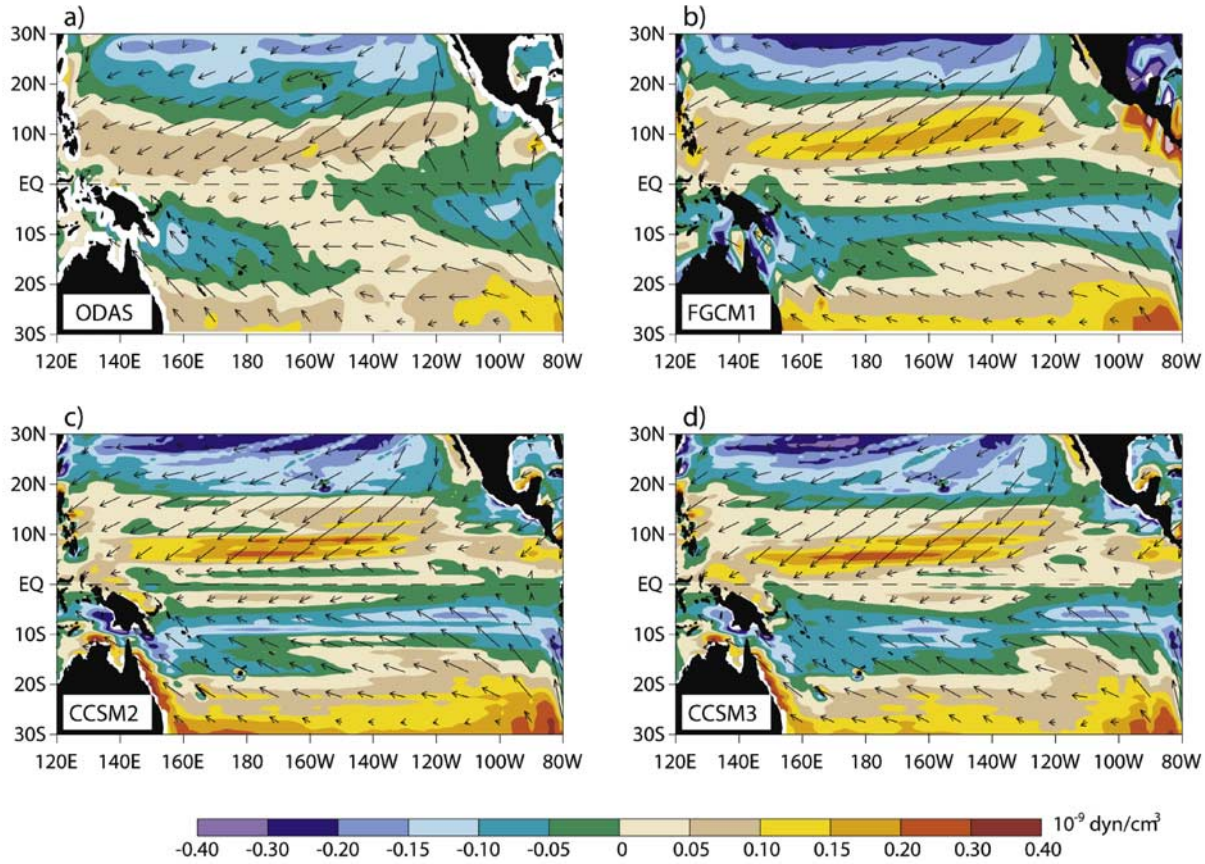

Figure 4. Annual mean wind stress curl (shaded, in 10^{-9} dyn/cm^3) and wind stress vector from (a) NCEP ODAS, (b) FGCM-1, (c) CCSM2, and (d) CCSM3.

in the previous subsection. This ridge is as strong as that associated with the ITCZ north of the Equator in FGCM-1 and CCSM2, and much stronger than its northern counterpart in CCSM3. The simulated subsurface ocean temperatures thus exhibit large cold biases at this latitude. These are consistent with work by *Kirtman et al.* [2002], *Zhang et al.* [2003], and *Kiehl and Gent* [2004]. The SST cold biases are seen at the equator. This is most clear in FGCM1 and CCSM2, less clear for CCSM3 because of the overall warm SST bias in this model. In companion with the symmetric structures of the ITCZ and SPCZ in the models, FGCM-1, CCSM2 and CCSM3 all simulated symmetric structures of thermocline and ocean currents to the Equator. The spurious ridge under the distorted SPCZ significantly intensified the SECC and displaced it to 5°S, making it connect with EUC and symmetric to its counterpart of the NECC. The intensified SECC has been also reported by *Terray* [1998] and *Zhang et al.* [2003].

[17] Except near the Equator, the controlling dynamic mechanism on the depth of the thermocline is Ekman pumping due to the surface wind curl. Positive wind curl in the Northern Hemisphere forces upwelling and ridging of the thermocline [*Kessler and Taft*, 1987]. In the Southern Hemisphere, negative curl forces upwelling because of the opposite sign of the Coriolis force.

[18] Figure 4a shows the surface wind vectors and their curls calculated from the NCEP ODAS in the equatorial Pacific. There are good correspondences between the ITCZ north of the Equator and the positive wind curl there, which corresponds well to the ridging of the thermocline in the western and central equatorial Pacific. South of the Equator, the maximum magnitude of the negative curl is located west of 140°W in the ODAS. Its orientation is very similar to that of the SPCZ, but its magnitude in the western and central equatorial Pacific is not as large as its counterpart north of the Equator. Ekman pumping is therefore weaker, and subsequently, the thermocline ridge is weak (Figure 3a).

[19] Different from observations, the FGCM-1, CCSM2, and CCSM3 all simulated structures of negative wind curls south of the Equator that are almost symmetric to their northern counterparts (Figures 4b–4d). The maximum magnitudes of the negative wind curls are located around 10°S, slightly south of the simulated SPCZ rainbands (Figures 1b–1d). They correspond well to the thermocline ridges shown in Figures 3b–3d. From the wind vectors in Figure 3, it is seen that the negative wind curl is mainly caused by the shear of the westward component of the southeast trade winds that approach the equator. Between 5°S–10°S and 180°–130°W, the simulated wind curls have opposite signs to observations. This is because the models failed to simulate the counterclockwise deflection of the southeast trade winds in this region – a consequence of the surface wind convergence toward the spurious rainband as discussed before. The band of negative wind curl extends eastward across the Pacific south of the Equator, causing ridging of the thermocline even in the Eastern Pacific, and

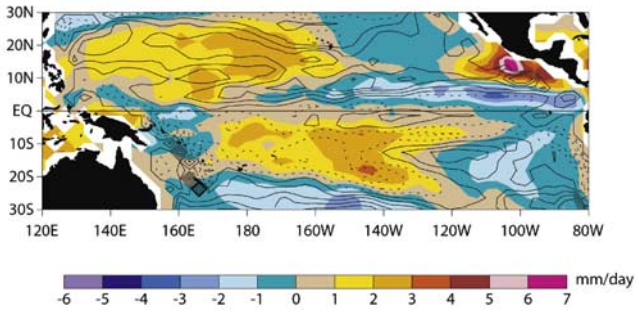

Figure 5. CAM3 annual mean biases of precipitation rate (shaded) and wind stress curl (contours, negative biases in dotted lines), with respect to COADS.

thus the strong South Equatorial Counter Current in the models.

[20] In the above discussions, we have used annual averages to show the double ITCZ structures in the central equatorial Pacific. Examination of their seasonal variations reveals that the above biases exist throughout the whole year. Even in the spring season from late February to early May when observations show double ITCZ of precipitation in the central Pacific, the models still significantly overestimate the intensity of precipitation south of the Equator.

3.3. Discussion

[21] The above analyses suggest a positive feedback mechanism in the coupled equatorial atmosphere-ocean system for the amplification of the double ITCZ symmetric structures in the coupled models relative to a stand-alone atmospheric model. We start by assuming an initial positive perturbation of precipitation in the models from 5°S–10°S at 180°E. The atmospheric latent heating associated with the precipitation anomaly then favors stronger convergence of surface winds toward the precipitation region (Figures 1 and 2). The changed wind pattern leads to anomaly of negative surface wind curl immediately south of the precipitation region due to the changed course of the southeast trade winds toward the precipitation region (Figure 4). The negative wind curl promotes Ekman pumping to cool the subsurface ocean, resulting in a thermocline ridge immediately south of the initial precipitation anomaly (Figure 3). The ridge then causes a meridional gradient in sea level, and hence a meridional upper ocean pressure gradient that drives stronger eastward SECC. This SECC coincides with the positive precipitation bias (Figures 1 and 3). When the SECC advects warm water eastward, positive SST anomaly will be formed at the eastern edge of the initial precipitation anomaly. This can move the initial precipitation perturbation further eastward. Meanwhile, air diverges from the equator toward the rainbands south and north of the Equator, leading to subsidence of air and upwelling of water at the equator to make the cold tongue moving westward.

[22] This feedback loop can therefore be described as through the chain of interactions of precipitation (latent heating), surface winds, wind curls, Ekman pumping, SSEC advection of ocean temperature, and SST. The specific configuration of the southeast trade winds in the South Pacific is a critical factor in this feedback process for the models because of the associated wind curls. There needs to be an initial perturbation to realize the positive feedback process. One of the plausible candidates is an initial bias of surface precipitation and wind curl in the stand-alone atmospheric models. It is widely known that atmospheric GCMs forced with observed SST contain signatures of the spurious eastward extension of the SPCZ, which is also associated with stronger surface southeast trade winds and biases of negative wind curls (e.g., Figure 5 from the uncoupled CAM3). It is not clear whether this is due to the lack of vertical transport of momentum by cumulus convections, or due to the overestimation of the trade winds in the atmospheric models. Another candidate of initial perturbation is a warm bias of sea surface temperature in the tropical southeastern Pacific due to the deficient amount of stratus clouds in the atmospheric model [*Yu and Mechoso*, 1999; *Dai et al.*, 2003].

[23] Schematics of the above processes are summarized in Figure 6. In Figure 6, we use the lightly shaded area to represent region of initial perturbation of precipitation. Surface winds are denoted by thin arrows, which have negative curls (curved arrows) south of the rain region. The curls force maximum upwelling and ridging at the latitude of the dashed line in Figure 6. This creates a meridional pressure gradient to produce the spurious SECC south of the equator (thick straight arrow). It advects warm water eastward and feedbacks to the initial precipitation.

4. Concluding Remarks

[24] We have shown that the three coupled models of CCSM2, CCSM3 and FGCM-1 all exhibit structures of the double ITCZs in terms of SST, surface precipitation, and surface winds that are too symmetric to the equator in the western and central equatorial Pacific that different from the ODAS data. These biases represent interaction of surface climate with atmospheric convection. They also project to the equatorial upper ocean: the surface wind convergences, associated with the zonally oriented double rainbands and SST maxima on both sides of the equator, also correspond to surface wind curls that are favorable to Ekman pumping immediately poleward of the rainbands. Thermocline ridges symmetric to the equator are then formed in the models that

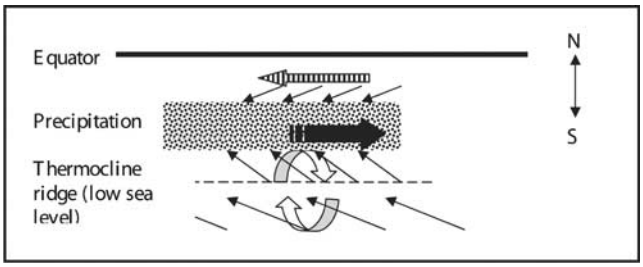

Figure 6. Schematic figure of key processes. Lightly shaded area represents region of initial precipitation. Thin arrows denote surface winds. Curved arrows denote negative curl. Dashed line is the latitude of thermocline ridging and thus low sea level height. The thick straight arrow represents the SECC forced by the meridional gradient of thermocline. The SECC advects warm water eastward.

cause significant overestimation of the South Equatorial Counter Current. These are shown to be in sharp contrast to observations in which the ITCZ in the north and the SPCZ in the south are highly asymmetric to the Equator in the western and central equatorial Pacific.

[25] A positive feedback mechanism is suggested to explain the amplification of the double ITCZs in coupled models through the following chain of interactions: surface precipitation, surface wind convergence, surface wind curl, Ekman pumping, thermocline ridging, SECC, eastward SST advection, warm SST, and precipitation. Initial trigger of this positive feedback process can be from biases in stand-alone atmospheric models in the equatorial Pacific which are known to exist, such as from cumulus convections or cloud simulations.

[26] Further study is needed to test the robustness of this positive feedback mechanism and to quantify it. Two lines of research are envisioned. One is to design controlled experiments of stand-alone and coupled models to examine the growing processes and the equilibrium states of the biases in the coupled models. The second is to construct mechanistic models to test the magnitude of the each feedback step by using available observations as constraints. A better understanding of this mechanism may lead to the development of new methodologies to suppress the spurious double ITCZ in coupled models. The present study is a first step toward this goal.

[27] **Acknowledgments.** We wish to thank Roberto Mechoso at UCLA and two anonymous reviewers for their constructive comments. This research is carried out while the first author was visiting Stony Brook University, which was partly sponsored by the Chinese Academy of Sciences. Additional support is provided by the U.S. Department of Energy, NASA, and the National Science Foundation to Stony Brook University. We wish to thank Wanqiu Wang at NCEP for helpful discussions. We also thank Yongqiang Yu and Weipeng Zheng for providing the FGCM-1 data and the NCAR CCSM project for providing the CCSM2 and CCSM3 data. NCAR is supported by the National Science Foundation.

References

Behringer, D. W., M. Ji, and A. Leetmaa (1998), An improved coupled model for ENSO prediction and implication for ocean initialization. part I: The ocean data assimilation system, *Mon. Weather Rev.*, *126*, 1013–1021.

Collins, W. D., et al. (2005), The Community Climate System Model CCSM3, *J. Clim.*, *19*, 2122–2143.

Covey, C., K. M. AchutaRao, U. Cubasch, P. Jones, S. J. Lambert, M. E. Mann, T. J. Phillips, and K. E. Taylor (2003), An overview of results from the Coupled Model Intercomparison Project, *Global Planet. Change*, *37*, 103–133.

Dai, F., R. Yu, X. Zhang, Y. Yu, and J. Li (2003), The impact of low-level cloud over the eastern subtropical Pacific on the ''double ITCZ'' in LASG FGCM-0, *Adv. Atmos. Sci.*, *20*(3), 461–474.

da Silva, A. M., C. C. Young, and S. Levitus (1994), *Atlas of Surface Marine Data 1994,* vol. 1, *Algorithms and Procedures*, *NOAA Atlas NESDIS*, vol. 6, 83 pp., NOAA, Silver Spring, Md.

Davey, M. K., et al. (2002), STOIC: A study of coupled model climatology and variability in tropical ocean regions, *Clim. Dyn.*, *18*, 403–420.

Guilyardi, E., P. Delecluse, S. Gualdi, and A. Navarra (2003), Mechanisms for ENSO phase change in a coupled GCM, *J. Clim.*, *16*, 1141–1158.

Ji, M., A. Leetmaa, and J. Derber (1995), An ocean analysis system for seasonal to interannual climate studies, *Mon. Weather Rev.*, *123*, 460–481.

Kessler, W. K., and B. A. Taft (1987), Dynamic heights and zonal geostrophic transports in the central tropical Pacific during 1979–84, *J. Phys. Oceanogr.*, *17*, 97–122.

Kiehl, J. T., and P. R. Gent (2004), The Community Climate System Model, version two, *J. Clim.*, *17*, 3666–3682.

Kirtman, B. P., Y. Fan, and E. K. Schneider (2002), The cola global coupled and anomaly coupled ocean–atmosphere GCM, *J. Clim.*, *15*, 2301–2320.

Latif, M., et al. (2001), ENSIP: The El Niño simulation intercomparison project, *Clim. Dyn.*, *18*, 255–276.

Liu, H.-L. (2002), High resolution oceanic general circulation model and the simulation of the upper ocean circulation in the tropical Pacific (in Chinese), Ph.D. thesis, 178 pp., Inst. of Atmos. Phys., Chin. Acad. of Sci., Taipei.

Ma, C.-C., C. R. Mechoso, A. W. Robertson, and A. Arakawa (1996), Peruvian stratus clouds and the tropical Pacific circulation: A coupled ocean–atmosphere GCM study, *J. Clim.*, *9*, 1635–1645.

Mechoso, C. R., et al. (1995), The seasonal cycle over the tropical Pacific in coupled ocean-atmosphere general circulation models, *Mon. Weather Rev.*, *123*, 3825–3838.

Meehl, G. A., and J. M. Arblaster (1998), The Asian-Australian monsoon and El Niño–Southern Oscillation in the NCAR climate system model, *J. Clim.*, *11*, 1356–1385.

Smith, R. D., and P. R. Gent. (Eds.) (2002), Reference manual for the Parallel Ocean Program (POP); ocean component of the Community Climate System Model (CCSM-2), Clim. and Global Dyn. Div., Natl. Cent. for Atmos. Res, Boulder, Colo. (Available at http://www.ccsm.ucar.edu/models/ccsm2.0.1/pop/.)

Terray, L. (1998), Sensitivity of climate drift to atmospheric physical parameterizations in a coupled ocean-atmosphere general circulation model, *J. Clim.*, *11*, 1633–1658.

Tomczak, M.. and J. S. Godfrey (2001), *Regional Oceanography: An Introduction*, Daya, Delhi. (Version 1.0 available at http://www.es.flinders.edu.au/~mattom/regoc/pdfversion.html.)

Waliser, D. E. (2003), Intertropical convergence zone, in *Encyclopedia of Atmospheric Sciences*, edited by J. R. Holton et al., pp. 2325–2334, Elsevier, New York.

Yu, J.-Y., and C. R. Mechoso (1999), Links between annual variations of Peruvian stratocumulus clouds and of SST in the eastern equatorial Pacific, *J. Clim.*, *12*, 3305–3318.

Yu, Y., R. Yu, X. Zhang, and H. Liu (2002), A flexible global coupled climate model, *Adv. Atmos. Sci.*, *19*, 169–190.

Yu, Y. Q., et al. (2005), *The Effect of Air-Sea Interaction on the Climate in China* (in Chinese), 201 pp., China Meteorol. Press, Beijing.

Zhang, C. (2001), Double ITCZs, *J. Geophys Res.*, *106*(D11), 11,785–11,792.

Zhang, M. H. (1996), Implication of the convection-evaporation-wind feedback to surface climate simulation in climate models, *Clim. Dyn.*, *12*, 299–312.

Zhang, X. H., Y. Yu, R. Yu, H. Liu, T. Zhou, and W. Li (2003), Assessments of an OGCM and the relevant CGCM. part I. Annual mean simulations in the tropical Pacific Ocean (in Chinese), *Sci. Atmos. Sin.*, *27*, 949–970.

W. Lin and M. Zhang, Institute for Terrestrial and Planetary Atmospheres, Stony Brook University, State University of New York, Stony Brook, NY 11794, USA. (mzhang@notes.cc.sunysb.edu)

X. Zhang, State Key Laboratory of Atmospheric Sciences and Geophysical Fluid Dynamics, Institute of Atmospheric Physics, Chinese Academy of Sciences, Beijing 100029, China.